

## Emission of particle unstable resonances from compound nuclei

M. A. Bernstein and W. A. Friedman

*Physics Department, University of Wisconsin, Madison, Wisconsin 53706*

W. G. Lynch

*National Superconducting Cyclotron Laboratory, Michigan State University, East Lansing, Michigan 48824*

(Received 20 July 1983)

The sequential emission and then decay of particle unstable resonances (such as  ${}^2\text{He}$ ) from compound nuclei is discussed. Calculations (based on a statistical model) of yields and energy spectra for the final stable products are presented. The effect of this sequential decay process on coincidence measurements is discussed.

### I. INTRODUCTION

The statistical model of Friedman and Lynch<sup>1</sup> predicts multiplicities and energy spectra for the evaporation of particles from compound nuclear systems. This model is flexible enough to permit calculation of the probability for evaporation of several unstable resonances as well as stable particles. We make use of this flexibility here to calculate the effects of these resonances on observable quantities. A different statistical method was employed earlier by Mekjian,<sup>2</sup> who also calculated some of these effects at higher energies. His results are sensitive to the thermodynamic volume parameter of his model.

Calculations based on the statistical model of Ref. 1 show that the multiplicities for evaporation of resonances such as  ${}^2\text{n}$ ,  ${}^2\text{He}$ ,  ${}^2\text{H}^*$  (the singlet state of the deuteron),  ${}^4\text{He}^*$ ,  ${}^5\text{He}$ , and  ${}^5\text{Li}$  can be significant. For example, the multiplicity of  ${}^2\text{He}$  can be of the order of 10% of the multiplicity of individual protons evaporated separately. Since each  ${}^2\text{He}$  decays into two secondary protons which are detected (the resonances dealt with here typically travel less than several hundred Fermis before decaying) such effects can be significant, especially in predictions of two-proton coincidence spectra or in the ratio of deuteron to proton yields. Moreover, the yield of protons and neutrons arising from the secondary decay of resonances can in some cases be 40% or more of the total evaporative yield for these particles.

In Sec. II we will describe a method for calculating the energy spectra of the final stable particles and show how the total yields are effected by secondary emission. In Sec. III we will use these spectra to construct coincidence cross sections and correlation functions. We will give sample

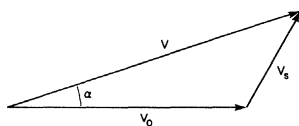


FIG. 1. Velocity diagram for the evaporation and subsequent decay of a resonance. The symbols are explained in the text.

calculations of some of these quantities.

In all the calculations below we include only particles resulting from evaporation of the compound nucleus. The calculations presented are for illustrative purposes. In subsequent papers, however, we will make direct comparisons with experimental data.

### II. CALCULATION OF SINGLES SPECTRA

In this section we will consider the emission and subsequent decay of a resonance from a compound nucleus, as shown in the velocity diagram Fig. 1. The velocity of the resonance (of mass  $m_0$ ) relative to the compound nucleus is  $\vec{v}_0$ . The resonance then decays into two secondary fragments, one of which has mass  $m$  and velocity  $\vec{v}_s$  relative to the frame of the resonance. We calculate the spectral distribution of the secondary as seen in the frame of the compound nucleus,  $dN_{ir}/dE$ , where  $E = \frac{1}{2}mv^2$ . This is normalized so that

$$\int_0^\infty \frac{dN_{ir}}{dE} dE = N_{ir}.$$

Here,  $N_{ir}$  is the average number of stable particles of type  $i$  which came from resonances of type  $r$ . We have

$$N_{ir} = N_r b_{ir},$$

where  $N_r$  is the average number of resonances of type  $r$  evaporated from the compound nucleus, and  $b_{ir}$  is the branching ratio. [For example, if the average number of  ${}^2\text{He}$  evaporated per compound nucleus were 0.17, then we would have  $N_{ir} = (0.17)(2) = 0.34$ .]

We first determine  $dN_{ir}/dE$  for all the resonances which yield stable particles of type  $i$ , and also determine the spectrum of particles of type  $i$  evaporated from the compound nucleus in one step,  $dN_{ci}/dE$ . Then the total spectrum of particle  $i$  is the sum

$$\frac{dN_i}{dE} = \frac{dN_{ci}}{dE} + \sum_r \frac{dN_{ir}}{dE}, \quad (1)$$

where  $dN_i/dE$  is the spectrum (in the frame of the compound system) of particles of type  $i$  to come from the

compound nucleus. Since we assume that  $\vec{v}_0$  (and also  $\vec{v}_s$ ) are isotropically distributed vectors,  $dN_i/dE$  will be isotropic in the compound system frame, and may be further transformed to the laboratory frame when the compound nucleus has a nonzero velocity. The transformation is accomplished by setting

$$\frac{d^2N_i}{dE_{\text{lab}}d\Omega_{\text{lab}}} = \frac{1}{4\pi} \left[ \frac{E_{\text{lab}}}{E} \right]^{1/2} \frac{dN_i}{dE}. \quad (2)$$

The statistical model of Ref. 1 supplies the important ingredients to calculate  $dN_i/dE$ . A computer program implementing it gives the spectra of the directly evaporated particles  $dN_{ci}/dE$  and also the spectra of resonances  $dN_r/dE_0$ , where  $E_0 = \frac{1}{2}m_0v_0^2$ . We can calculate the normalized spectrum of particles of type  $i$  to come from resonances of type  $r$ ,  $(db_{ir}/dE)(E_0)$ , if we are given a value of  $E_0$  and some distribution for  $E_s$ . If this spectrum is subject to the normalization

$$\int_E \frac{db_{ir}}{dE}(E_0)dE = b_{ir} \text{ (for all } E_0),$$

then

$$\frac{dN_{ir}}{dE} = \int_{E_0} \frac{db_{ir}}{dE}(E_0) \frac{dN_r}{dE_0} dE_0.$$

To calculate  $(db_{ir}/dE)(E_0)$ , note that for any value of  $\vec{v}_0$

$$\frac{d^3b_{ir}}{d^3\vec{v}} = \frac{d^3b_{ir}}{d^3\vec{v}_s}.$$

Since  $\vec{v}_s$  is assumed to be isotropic

$$\frac{db_{ir}}{dE}(E_0) = \frac{1}{2} \int_{-1}^1 \left[ \frac{E}{E_s} \right]^{1/2} \frac{db_{ir}}{dE_s} d(\cos\alpha), \quad (3)$$

where

$$E_s = E + \frac{m}{m_0}E_0 - 2 \left[ EE_0 \frac{m}{m_0} \right]^{1/2} \cos\alpha.$$

For some line shapes  $db_{ir}/dE_s$ , the integral (3) may be evaluated analytically. For example, it is well known that if  $db_{ir}/dE_s = b_{ir}\delta(E_s - \mu)$ , then the graph of  $(db_{ir}/dE)(E_0)$  vs  $E$  has the shape of a box. If the resonant energy is  $\xi$  and the full width at half maximum (FWHM) is  $\Gamma$ , then we can consider the Lorentzian

$$\frac{db_{ir}}{dE_s} = \theta(E_s) \left[ \frac{b_{ir}}{\pi/2 + \tan^{-1}(2\mu/\Delta)} \right] \times \left[ \frac{\Delta/2}{(E_s - \mu)^2 + (\Delta/2)^2} \right], \quad (4)$$

where to correct for recoil,<sup>1</sup> we set

$$\mu = \xi \left[ \frac{m_0 - m}{m_0} \right],$$

$$\Delta = \Gamma \left[ \frac{m_0 - m}{m_0} \right].$$

The substitution of Eq. (4) into Eq. (3) allows  $(db_{ir}/dE)(E_0)$  to be evaluated analytically.<sup>3</sup>

If both secondary particles have charge, then Eq. (4) may be unsuitable because the Coulomb repulsion will tend to suppress  $db_{ir}/dE_s$  for small values of  $E_s$ . In this case we instead use a Maxwell-Boltzmann line shape

$$\frac{db_{ir}}{dE_s} = \frac{2b_{ir}}{\pi^{1/2}G^{3/2}} \theta(E_s - V)(E_s - V)^{1/2} e^{-(E_s - V)/G}, \quad (5)$$

where we set

$$G \simeq \frac{\Gamma}{1.795} \left[ \frac{m_0 - m}{m_0} \right],$$

$$V = \xi \left[ \frac{m_0 - m}{m_0} \right] - \frac{G}{2},$$

because in Eq. (5) the peak value occurs at  $V + G/2$  and the full width at half maximum is approximately 1.795 G. When Eq. (5) is inserted in Eq. (3),  $(db_{ir}/dE)(E_0)$  can be obtained by numerical integration.

For the purpose of generating the resonant contribution to the singles spectra we use experimental data to estimate  $\xi$  and  $\Gamma$  which are used in Eqs. (4) and (5). For  $A=2$  resonances, low-energy phase shift data is available.<sup>4</sup> Neglecting the possible effects of the Coulomb field from the compound nucleus, we follow the theory of final state interactions,<sup>5</sup> and estimate  $\Gamma$  and  $\xi$  from the shape of the spectral distribution

$$\frac{\sin^2\delta(k)}{k}, \quad (6a)$$

where  $\delta(k)$  is the phase shift and  $\hbar k$  is the relative momentum. Similarly, for  ${}^2\text{He}$  we use the modified<sup>6</sup> line shape

$$\frac{\eta}{e^{2\pi n} - 1} \frac{\sin^2\delta(k)}{k}, \quad (6b)$$

where  $\eta$  is the Sommerfeld parameter.

For the  $A=5$  resonances ( ${}^5\text{Li}$  and  ${}^5\text{He}$ ), the value of  $\xi$  is taken to be the  $Q$  value for the reaction, and  $\Gamma$  from tables.<sup>7</sup> The  ${}^4\text{He}^*$  assumed to be composed of several excited states and capable of decay into the  $n, {}^3\text{He}$  or  $p, {}^3\text{H}$

TABLE I. Decay channels and values of decay parameters for the resonances considered in this paper.  $b_{ir}$  is the branching ratio, and  $\xi$  and  $\Gamma$  are the resonant energy and full width at half maximum, respectively.

Resonance ( $r$ )	Particle ( $i$ )	$b_{ir}$	$\xi, \Gamma$ (MeV)
${}^2\text{He}$	p	2	0.8, 2.8
${}^2\text{H}^*$	p or n	1	0.07, 0.5
${}^2\text{N}$	n	2	0.12, 1.0
${}^4\text{He}^*$	p or ${}^3\text{H}$	0.33	0.8, 1.0
${}^4\text{He}^*$	n or ${}^3\text{He}$	0.67	1.1, 1.0
${}^5\text{Li}$	p or ${}^4\text{He}$	1	1.97, 1.5
${}^5\text{He}$	n or ${}^4\text{He}$	1	0.893, 0.60

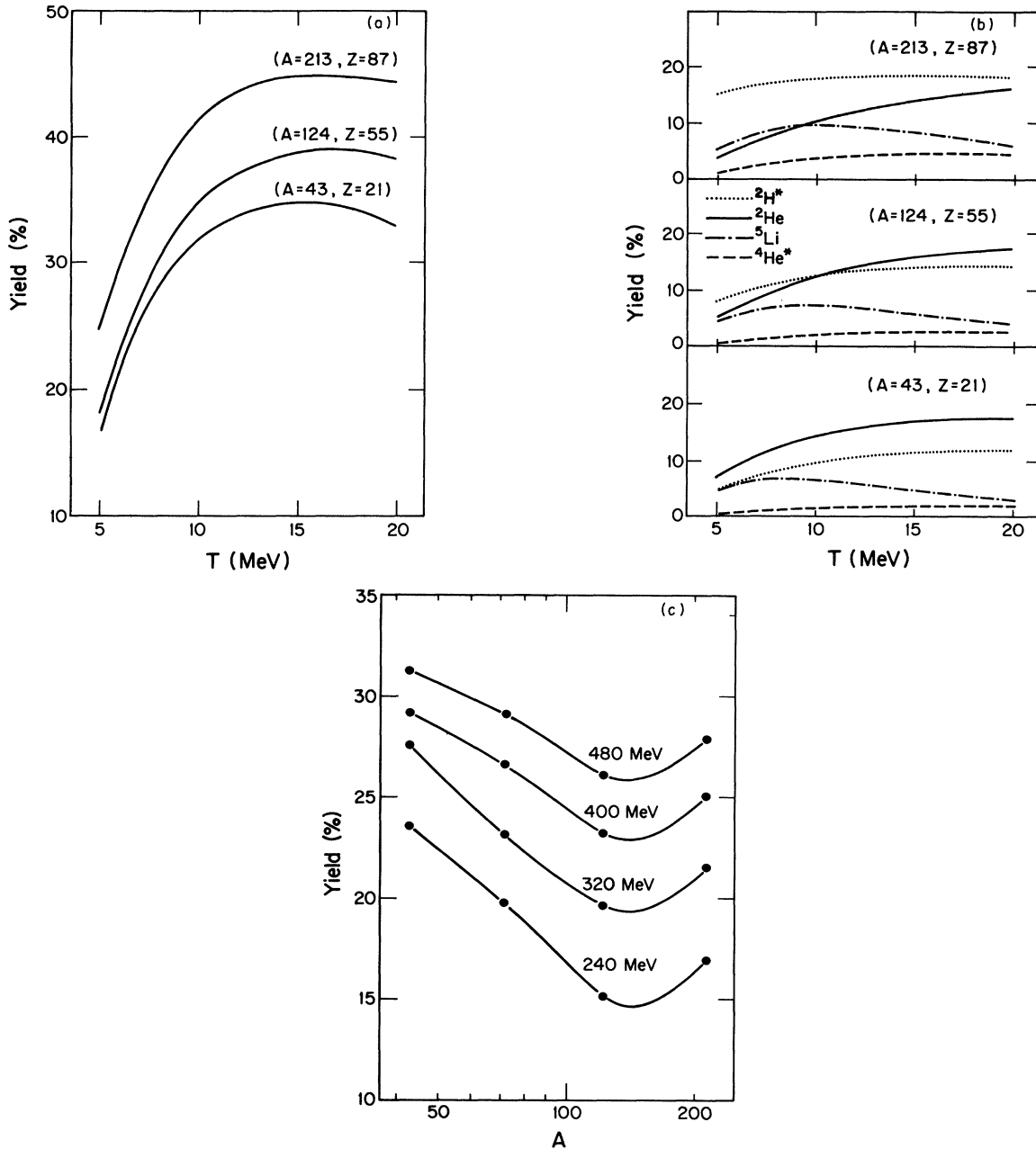


FIG. 2. Percentage of the total proton yield coming from the  ${}^2\text{H}^*$ ,  ${}^2\text{He}$ ,  ${}^4\text{He}^*$ , and  ${}^5\text{Li}$  resonances. (a) shows this percentage vs maximum compound nuclear temperature for three different compound systems. (b) shows the partial percentages contributed by the various resonances. (c) shows the total percentage as a function of compound nuclear mass. The lines represent a given laboratory energy for an  ${}^{16}\text{O}$  beam and the points represent the targets  ${}^{27}\text{Al}$ ,  ${}^{56}\text{Fe}$ ,  ${}^{107}\text{Ag}$ , and  ${}^{197}\text{Au}$ . Intermediate points (not shown) can deviate from the lines by a few percent of the yield.

channels. The values of  $b_{ir}$ ,  $\Gamma$ , and  $\xi$  are roughly estimated from scattering data.<sup>8</sup> Table I summarizes the values of the parameters used in this calculation.

Some of the systematic effects of secondary emission on the yield of protons is shown in Fig. 2. For a given initial compound nuclear temperature, Fig. 2(a) shows that the fraction of evaporated protons to come from resonances increases with the mass of the compound nucleus. This is mostly due to our choice for the Fermi energy, which is

an important input to the statistical model. For the  $A=43$ , 124, and 213 systems, we use Fermi energies of 25, 30, and 38 MeV, respectively. Figure 2(b) shows the secondary contribution to the proton spectrum broken down according to the various resonances. The  ${}^2\text{H}^*$  and the  ${}^2\text{He}$  give the greatest contributions, with the competition between these two strongly influenced by the Coulomb barrier, especially at the lower temperatures.

Figure 2(c) shows the contribution to the proton yield

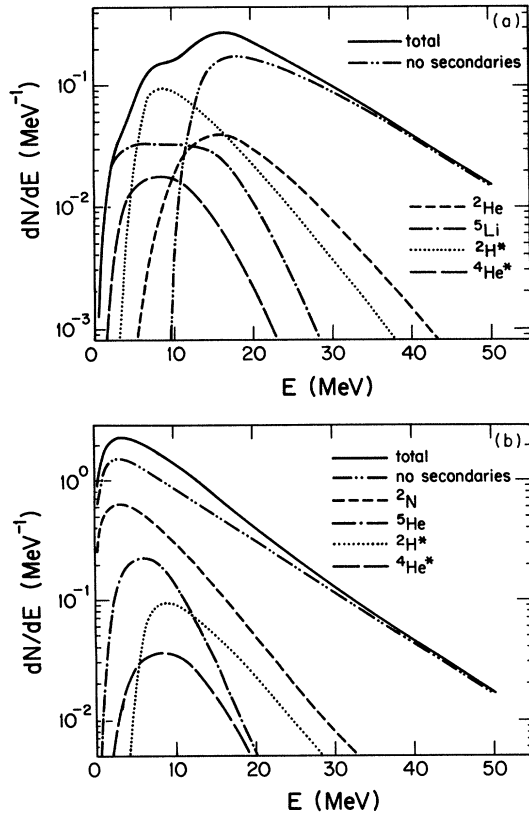


FIG. 3. Spectrum of evaporated protons (a) and neutrons (b) in the compound nuclear frame. The contributions from the various resonances are shown. The compound system has  $A=213$ ,  $Z=87$  and a maximum temperature of 10 MeV. Because of secondary emission, protons appear below the primary Coulomb barrier and neutrons appear above the thermal peak.

from secondaries as a function of compound nuclear mass for a fixed energy projectile. In this graph the lines represent a given laboratory energy for an  $^{16}\text{O}$  beam, and the points are compound nuclear systems formed by fusing  $^{16}\text{O}$  and various targets. For small  $A$ , the curves have a negative slope because the temperature drops sharply with increasing  $A$ . For larger  $A$ , this decrease in temperature is more than offset by the Fermi energy effect discussed in connection with Fig. 2(a).

Figure 3(a) shows a  $dN_p/dE$  (in the compound nuclear frame) calculated by Eq. (1) for evaporation of protons from  $^{16}\text{O}$  fused with  $^{197}\text{Au}$  having an initial temperature of 10 MeV. Note that some protons are predicted below the primary Coulomb barrier. To understand this, consider the evaporation of a  $^2\text{H}^*$ . When the temperature is not too high, a significant amount of the  $^2\text{H}^*$  kinetic energy will come from acceleration in the Coulomb field of the compound nucleus. But when the  $^2\text{H}^*$  decays the proton and neutron share this energy. This same effect can be seen to produce neutrons at energies above the thermal peak in Fig. 3(b). Figure 4 shows proton and neutron spectra from a less highly charged system,  $^{16}\text{O}$  fused with  $^{27}\text{Al}$ , also with an initial temperature of 10 MeV. With the lower Coulomb barrier, the energies of the protons and

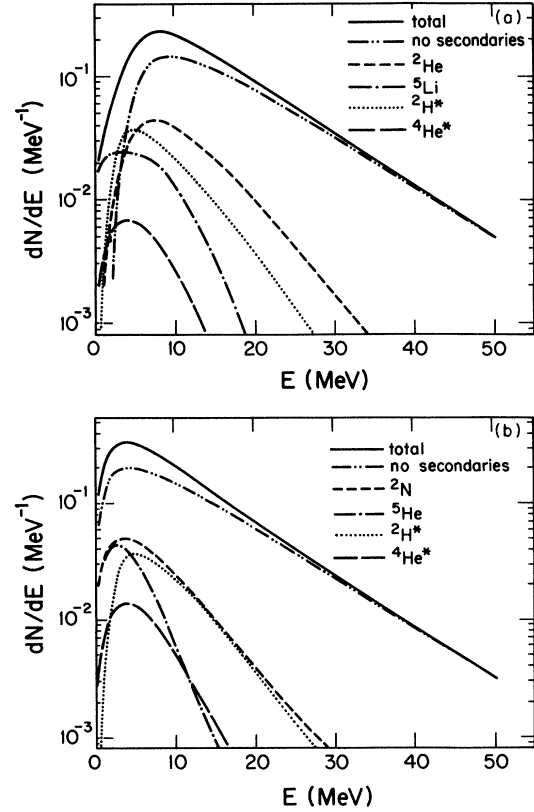


FIG. 4. Spectrum of evaporated protons (a) and neutrons (b) in the compound nuclear frame. The compound system has  $A=43$ ,  $Z=21$  and a maximum temperature of 10 MeV.

neutrons coming from resonances are essentially the same as those which evaporate in one step.

### III. CALCULATION OF COINCIDENCE SPECTRA

A more direct consequence of the evaporation of unstable resonances from the compound nucleus is given by the coincidence signatures of these events.<sup>9</sup> In this section we calculate coincidence quantities from the results obtained in Sec. II.

Figure 5 shows a velocity diagram for a sequential decay. The velocity of the compound nucleus relative to the laboratory frame is  $\vec{v}_c$ . As before,  $\vec{v}_0$  is the velocity of the

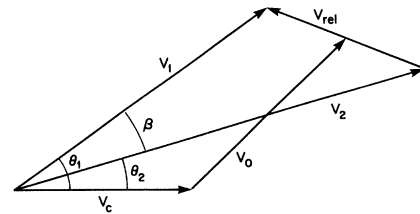


FIG. 5. Velocity diagram for the evaporation and subsequent decay of a resonance into two fragments of equal mass. The symbols are explained in the text.

resonance relative to the compound nucleus, and  $\vec{v}_{\text{rel}}$  is the relative velocity between the two fragments. Fragment 1 has a laboratory velocity of  $\vec{v}_1$  and lands in detector 1 at laboratory angles  $\theta_1$  and  $\phi_1$ , and similarly for fragment 2. If we specialize to the important special case where  $m_1 = m_2 = m$ ,

$$\begin{aligned}\vec{v}_1 &= \frac{1}{2}\vec{v}_{\text{rel}} + \vec{v}_0 + \vec{v}_c, \\ \vec{v}_2 &= -\frac{1}{2}\vec{v}_{\text{rel}} + \vec{v}_0 + \vec{v}_c.\end{aligned}\quad (7)$$

In accordance with Fig. 5 we can also define

$$E_1 = \frac{1}{2}mv_1^2, \quad E_2 = \frac{1}{2}mv_2^2,$$

and

$$\begin{aligned}E_{\text{rel}} &= \frac{1}{2}[E_1 + E_2 - 2(E_2 E_1)^{1/2} \cos \beta], \\ E_0 &= \frac{1}{2}[E_1 + E_2 + 2(E_1 E_2)^{1/2} \cos \beta] \\ &\quad + v_c[mv_c - (2mE_1)^{1/2} \cos \theta_1 - (2mE_2)^{1/2} \cos \theta_2], \\ \cos \beta &= \cos \theta_1 \cos \theta_2 + \sin \theta_1 \sin \theta_2 \cos(\phi_1 - \phi_2).\end{aligned}$$

It will be convenient in this section to define a general normalized distribution

$$f(x_1, x_2, \dots, x_k) \equiv \frac{1}{N} \frac{d^k N}{dx_1 dx_2 \cdots dx_k},$$

so that

$$\int f(x_1, x_2, \dots, x_k) dx_1 dx_2 \cdots dx_k = 1.$$

Equation (7) gives

$$d^3 \vec{v}_1 d^3 \vec{v}_2 = d^3 \vec{v}_{\text{rel}} d^3 \vec{v}_0,$$

since  $\vec{v}_c$  is a constant, so that

$$f(\vec{v}_1, \vec{v}_2) = f(\vec{v}_{\text{rel}}, \vec{v}_0).$$

But if we assume independence of the distributions for the vectors  $\vec{v}_{\text{rel}}$  and  $\vec{v}_0$ , then

$$f(\vec{v}_{\text{rel}}, \vec{v}_0) = f(\vec{v}_{\text{rel}})f(\vec{v}_0).$$

This leads to

$$f(E_1, E_2, \Omega_1, \Omega_2) = \left[ \frac{1}{4\pi} \right]^2 \left[ \frac{E_1 E_2}{E_{\text{rel}} E_0} \right]^{1/2} f(E_{\text{rel}})f(E_0). \quad (8)$$

Thus, the differential coincidence probability  $f(E_1, E_2, \Omega_1, \Omega_2)$  is expressed in Eq. (8) entirely in terms of laboratory quantities and calculable spectra. According to the definition of the  $f$ 's we have

$$\int f(E_1, E_2, \Omega_1, \Omega_2) dE_1 dE_2 d\Omega_1 d\Omega_2 = 1.$$

To calculate the average number of coincidence counts per  $(\text{MeV}^2 \text{sr}^2)$  per compound nucleus at a given  $(E_1, E_2, \Omega_1, \Omega_2)$ , we must include counts in addition to those represented by Eq. (8). The counts from the latter equation arise from fragment particles (say protons) which both came from a single resonant particle (a specific  ${}^2\text{He}$ ), as shown in Fig. 5. However, we can also have two pro-

tons evaporated completely independently from the same compound nucleus, which are detected in coincidence. Let  $N_{\text{He}}$  and  $N_p$  be the total multiplicities of  ${}^2\text{He}$  and protons, respectively, and  $f_p(E_1, \Omega_1)$  be the proton spectrum [Eq. (2) at detector 1, normalized to unity].

We construct the quantity  $n_{\text{He}}(1,2)$  equal to the total number of coincidence counts per  $(\text{MeV}^2 \text{sr}^2)$  per compound nucleus when the detectors look for coincidences at  $(E_1, E_2, \Omega_1, \Omega_2)$ .  $n_{\text{He}}(1,2)$  should contain a term

$$2N_{\text{He}}f(E_1, E_2, \Omega_1, \Omega_2),$$

to represent the coincidences which stem from a single  ${}^2\text{He}$ . We also wish to normalize

$$\int n_{\text{He}}(1,2) dE_1 dE_2 d\Omega_1 d\Omega_2 = N_p(N_p - 1),$$

because this is the maximum number of coincidences (twice the number of pairs) if no proton can enter both detectors. We can therefore approximate  $n_{\text{He}}$  with the simple form

$$\begin{aligned}n_{\text{He}}(1,2) &= [N_p(N_p - 1) - 2N_{\text{He}}]f_p(E_1, \Omega_1)f_p(E_2, \Omega_2) \\ &\quad + 2N_{\text{He}}f(E_1, \Omega_1, E_2, \Omega_2).\end{aligned}\quad (9)$$

If we know the cross section for compound nucleus formation  $\sigma_0$ , then we can transform  $n_{\text{He}}(1,2)$  into a cross section

$$\frac{d^4 \sigma}{dE_1 dE_2 d\Omega_1 d\Omega_2} = \sigma_0 n_{\text{He}}(1,2). \quad (10)$$

We can also transform  $n_{\text{He}}(1,2)$  into a dimensionless correlation function  $C_{\text{He}}(1,2)$ ,

$$C_{\text{He}}(1,2) = \frac{n_{\text{He}}(1,2)}{N_p^2 f_p(E_1, \Omega_1) f_p(E_2, \Omega_2)}. \quad (11)$$

This correlation function differs from the one calculated by Koonin.<sup>10</sup> The latter does not include sequential decay of unstable resonances, and primarily gives informa-

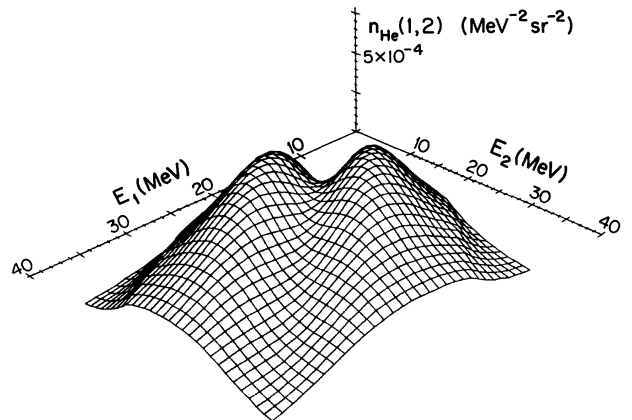


FIG. 6. Number of p-p coincidence counts per  $(\text{MeV}^2 \text{sr}^2)$  per compound nucleus vs laboratory energies  $E_1$  and  $E_2$ , for laboratory angles  $\theta_1 = \theta_2 = 25^\circ$  and  $\beta = 5^\circ$ . The compound system is formed by fusing 400 MeV  ${}^{16}\text{O}$  with  ${}^{12}\text{C}$ .  $E_1$  and  $E_2$  take on values between 11 and 40 MeV.

tion about the temporal and spatial size of the interaction region. The correlation function given by Eq. (11), however, neglects the interactions among particles evaporated independently, which we assume are events well separated in time.

Figure 6 shows a plot of  $n_{\text{He}}(1,2)$  (for protons) vs  $E_1$  and  $E_2$  for the example of a compound system formed by fusing 400 MeV  $^{16}\text{O}$  with  $^{12}\text{C}$ . The laboratory angles are  $\theta_1=\theta_2=25$ , and  $\beta=5^\circ$ . One advantage of using a light compound nuclear system was suggested by Fig. 2(b)—a large Coulomb barrier tends to inhibit  $^2\text{He}$  production, especially at the lower temperatures. In this example, the statistical calculation gives  $N_{\text{He}}=0.162$ ,  $N_p=2.43$ , and a maximum compound nuclear temperature of 9.4 MeV. If we assume a geometrical value for  $\sigma_0$ , then the peaks in Fig. 6 correspond to a value of about 0.2 mb/MeV $^2$ sr $^2$  for the coincidence cross section in Eq. (10). The valley along the line  $E_1=E_2$  is mostly due to the Coulomb repulsion of the two protons, and deepens very rapidly as the opening angle  $\beta$  is decreased.

Because the line shape  $f(E_{\text{rel}})$  is critical for these plots we used a better fit to Eq. (6b) than is supplied by Eq. (5). Experimental data<sup>11</sup> suggest that the final state interaction formalism is valid up to relative energies of at least 2 MeV. We therefore take

$$f(E_{\text{rel}}) = \begin{cases} a \left[ \frac{\eta}{e^{2\pi\eta} - 1} \right] \frac{\sin^2\delta(k)}{k}, & E_{\text{rel}} \leq 2.0 \text{ MeV} \\ b \exp(-cE_{\text{rel}}), & E_{\text{rel}} > 2.0 \text{ MeV} \end{cases} \quad (12)$$

where  $a$  and  $b$  are chosen so that  $f(E_{\text{rel}})$  is both normalized and continuous at  $E_{\text{rel}}=2.0$  MeV, and  $c$  is a free parameter that we have set equal to 1 MeV $^{-1}$ .

In a similar way, we can study the effect of the  $^2\text{H}^*$  resonance on n-p coincidence spectra. If we specify that the neutron enters detector 1, we can modify Eq. (9) to give the number of n-p coincidence counts,  $n_D(1,2)$ . We take

$$n_D(1,2) = (N_n N_p - N_D) f_n(E_1, \Omega_1) f_p(E_2, \Omega_2) + N_D f(E_1, \Omega_1, E_2, \Omega_2),$$

where  $N_n$  and  $N_D$  are the number of neutrons and  $^2\text{H}^*$  resonances evaporated per compound nucleus, and  $f_n(E_1, \Omega_1)$  is the neutron spectrum [Eq. (2) at detector 1, normalized to unity].

Figure 7 shows  $n_D(1,2)$  for 420 MeV  $^{14}\text{N}$  on  $^{197}\text{Au}$  at  $\theta_1=\theta_2=60^\circ$  and  $\beta=2^\circ$ . Here, the statistical model predicts  $N_n=18.1$ ,  $N_p=1.05$ , and  $N_D=0.164$ , and a maximum compound nuclear temperature of 5.3 MeV. For  $f(E_{\text{rel}})$ , we use a line shape similar to Eq. (12), except the Coulomb suppression factor is absent. If we again assume a geometrical value for  $\sigma_0$ , then the peaks in Fig. 7 correspond to a coincidence cross section value of about 1.4 mb/MeV $^2$ sr $^2$ . Note that the peaks in Fig. 7 occur at a lower energy than those in Fig. 6, primarily because the compound nucleus has a smaller speed relative to the laboratory. The valley along the line  $E_1=E_2$  is due to the phase space suppression of the quantity in Eq. (6a) for small values of  $k$ . The background is asymmetric because the Coulomb field of the compound nucleus inhibits evaporation of low energy protons.

Finally, we will mention several interesting effects that may occur in the case of the  $^2\text{H}^*$ . If the resonance decays while it is still in the strong Coulomb field of the compound nucleus then the proton will gain an additional amount of energy relative to the neutron. If the  $^2\text{H}^*$  decays a distance  $r$  from the compound nucleus then

$$\Delta E = \frac{Z_c e^2}{r},$$

where  $Z_c$  is the charge for the compound nucleus averaged over the evaporation process. We have

$$r \simeq \left( \frac{E_0}{m} \right)^{1/2} \frac{\hbar}{\Gamma},$$

the product of the speed and lifetime of the resonance. Putting  $Z_c=50$  and  $\Gamma=0.5$  MeV we obtain

$$\Delta E \simeq \frac{6 \text{ MeV}^{3/2}}{E_0^{1/2}}.$$

Also, the tidal force of Coulomb repulsion may polarize the  $^2\text{H}^*$  and may cause it to disintegrate before its free lifetime of  $\hbar/\Gamma$ . This premature breakup would cause collision broadening of the line shape, thus increasing  $\Gamma$  and  $\Delta E$ , but smearing out the structure in Fig. 7 somewhat. This polarization may align  $\vec{v}_{\text{rel}}$  along the direction of  $\vec{v}_0$ , and thus invalidate the condition of independence of these two vectors. We plan to treat the  $^2\text{H}^*$  resonance in more detail in future papers.

#### IV. CONCLUSION

We have presented some of the systematic effects of secondary emission on proton yields. The mathematics necessary for computing both singles and coincidence spectra for emission from compound nuclear systems when unstable resonances are present have been described.

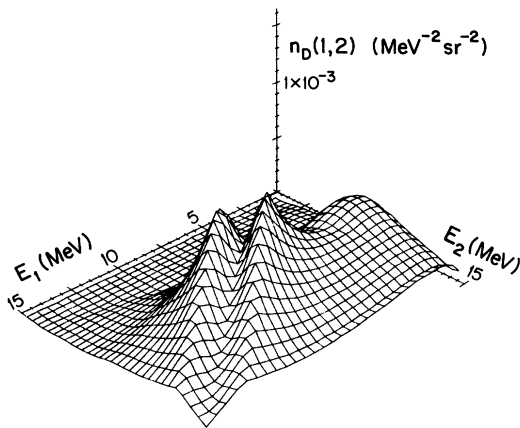


FIG. 7. Number of n-p coincidence counts per (MeV $^2$ sr $^2$ ) per compound nucleus vs laboratory energies  $E_1$  and  $E_2$  ( $E_1$  is the neutron energy). The laboratory angles are  $\theta_1=\theta_2=60$  and  $\beta=2^\circ$ . The compound system is formed by fusing 420 MeV  $^{14}\text{N}$  with  $^{197}\text{Au}$ .  $E_1$  and  $E_2$  take on values between 0.5 and 15 MeV.

Illustrative examples of spectra have shown emission of protons below the Coulomb barrier, and neutrons above the thermal peak, especially from high- $Z$  systems. Other calculations show how unstable resonances can leave "fingerprints" on a coincidence spectra, even if relatively few of the resonances are evaporated. In future papers we

will compare the results of our calculations with experimental data.

This work was supported by the National Science Foundation under grants Nos. PHY 82-04302 and PHY 80-17605.

---

<sup>1</sup>W. A. Friedman and W. G. Lynch, Phys. Rev. C 28, 16 (1983).

<sup>2</sup>A. Z. Mekjian, Phys. Rev. C 17, 1051 (1978).

<sup>3</sup>The substitution  $w = E_s^{1/2}$  leads to an integral which is in tables. See, for example, integral 2.161 in I. S. Gradshteyn and I. M. Ryzhik, *Table of Integrals, Series and Products* (Academic, New York, 1980), p. 67.

<sup>4</sup>H. P. Noyes and H. M. Lipinski, Phys. Rev. C 4, 995 (1971).

<sup>5</sup>K. M. Watson, Phys. Rev. 88, 1163 (1952).

<sup>6</sup>A. B. Migdal, Zh. Eksp. Teor. Fiz. 28, 3 (1955) [Sov. Phys.—JETP 1, 2 (1955)]. A concise review of the elements of final state interaction theory that we use here is given by R. J. N.

Phillips, Nucl. Phys. 53, 650 (1964).

<sup>7</sup>F. Ajzenberg-Selove, Nucl. Phys. A320, 1 (1979).

<sup>8</sup>S. Fiarman and W. E. Meyerhof, Nucl. Phys. A206, 1 (1973).

<sup>9</sup>See, for example, M. D. Cable *et al.*, Phys. Rev. Lett. 50, 404 (1983), for a report of the discovery of beta-delayed two-proton radioactivity for the power of the correlation technique in a related problem.

<sup>10</sup>Steven E. Koonin, Phys. Lett. 70B, 43 (1977).

<sup>11</sup>J. van Driel, R. Kamermans, R. J. de Mijeer, and A. E. L. Dieperink, Nucl. Phys. A342, 1 (1980).